2-17-2012

Excessive Grain Boundary Conductivity of Spin-Spray Deposited Ferrite/Non-Magnetic Multilayer

Yun Xing
Wright State University - Main Campus

J. Myers
Wright State University - Main Campus

Ogheneyunume Obi
Northeastern University

Nian X. Sun
Northeastern University

Yan Zhuang
Wright State University - Main Campus, yan.zhuang@wright.edu

Excessive grain boundary conductivity of spin-spray deposited ferrite/non-magnetic multilayer

Yun Xing,[1,a)] J. Myers,[1] Ogheneyunume Obi,[2] Nian X. Sun,[2] and Yan Zhuang[b)]
[1]*Department of Electrical Engineering, Wright State University, Dayton, Ohio 45435, USA*
[2]*Department of Electrical and Computer Engineering, Northeastern University, Boston, Massachusetts 02115, USA*

(Presented 31 October 2011; received 12 September 2011; accepted 10 November 2011; published online 17 February 2012)

Magnetic materials with a high self-biased ferromagnetic resonance (FMR) frequency and low electrical conductivity hold great potential for RF/microwave devices. In this work, ferrite film consisting of Fe_3O_4 (1.2 μm)/photoresist (60 nm)/Fe_3O_4 (1.2 μm) was deposited at 90 °C via spin spray deposition. Broadband impedance imaging with nanometer spatial resolution was recorded by using scanning microwave microscopy. Compared to a reference sample, it turned out that the grain boundary appeared to be more conductive than the grain. © *2012 American Institute of Physics*. [doi:10.1063/1.3676242]

I. INTRODUCTION

Governed by the Landau-Lifshitz equation,[1] the magnetic permeability is mainly determined by the saturation magnetization, ferromagnetic resonant frequency, magnetic anisotropic field, damping factor, external magnetic field, and shape-induced demagnetizing factor. Apart from these, the conductivity of the magnetic material and the induced eddy current at radio frequency (RF)/microwave frequencies deteriorate the magnetic permeability and significantly increase the loss. In fact, the high conductivity imposes a formidable challenge in applying metallic ferromagnetic thin films in integrated RF/microwave circuits, though many efforts have been made to develop high resistivity magnetic nano-granular films.[2–7]

Low temperature spin sprayed ferrite films (Fe_3O_4) with high self-biased ferromagnetic resonance (FMR) frequency and high electrical resistivity have been recently reported.[8] Such films can find immediate applications in patch antennas and bandpass filters.[9,10] However, the spin sprayed Fe_3O_4 films suffer from a high magnetic loss.

In this study, broadband impedance imaging with nanometer spatial resolution was recorded using scanning microwave microscopy (SMM). The imaging contrast revealed the difference in the electrical properties of the grain boundary and of the inner grains. It turned out that the grain boundary of the spin sprayed Fe_3O_4 films had a higher electrical conductivity than the inner grains.

II. EXPERIMENTS

The Fe_3O_4 (1200 nm)/photoresist (PR 30 nm)/Fe_3O_4 (1200 nm) multilayer thin film was fabricated at 90 °C via spin spray deposition onto commercially available 0.1 mm thick glass substrate. An oxidation solution containing 2 mM $NaNO_2$ and 140 mM CH_3COONa with a *p*H value of 9 and a precursor solution containing 10 mM Fe^{2+} and a *p*H of 4 were sprayed simultaneously through two separate nozzles onto a glass substrate rotating at 145 rpm in the presence of N_2 gas. The growth rate was ~40 nm/min.

The magnetic properties of the film were measured using a vibrating sample magnetometer (VSM) with an external magnetic field applied parallel (in-plane) and perpendicular (out of plane) to the film plane. The FMR spectrum of the film was determined using an electron paramagnetic resonance (EPR) system operating at X-band (9.6 GHz) with an external magnetic field applied parallel to the film plane, and the complex permeability spectra of the film was measured using a broad band custom-made permeameter consisting of a coplanar waveguide connected to a network analyzer with a bandwidth of 0.045 to 10 GHz. The structural and magnetic properties are summarized in Table I.

SMM consists of an atomic force microscope (AFM) and a microwave network analyzer (PNA). Such a system allows the simultaneous characterization of the surface morphology and electromagnetic properties of the sample. The lateral resolution of SMM is proportional to the tip radius, and its principle has been described recently.[11–13] For comparison, a reference sample with a 5 nm thick partially oxidized graphene nanosheet on a platinum surface was measured.

III. RESULTS AND DISCUSSION

The complex magnetic permeability of the Fe_3O_4/PR/Fe_3O_4 multilayer was measured and shown in Fig. 1. Simulations were performed based on the parameters listed in Table I. The Landau-Lifshitz phenomenological damping constant α was assumed to be ~0.46 in the simulation in order to obtain a reasonable fit. The value is, however, far above the value of ~0.011 obtained from the EPR in Table I. This is partly because the broad band complex permeability measurement was done in the absence of external magnetic field, whereas the EPR measurement was performed in a strong

[a)]Current address: Department of Engineering Physics, Air Force Institute of Technology, Wright-Patterson AFB, Ohio 45433, USA.
[b)]Author to whom correspondence should be addressed. Electronic mail: yan.zhuang@wright.edu. FAX: 001-937-775-3936.

TABLE I. Summary of film structural and magnetic properties (saturation magnetization M_s, coercivity H_c, real permeability at 300 MHz μ_r', and FMR linewidth ΔH at X-band (9.6 GHz)) of the ferrite/non-magnetic multilayers.

Film structure	Thickness (μm)	M_s (emu/cm^3)	H_k (Oe)	μ_r'	ΔH (Oe)	ρ (Ω cm)
Fe_3O_4/PR/Fe_3O_4	2.4	183.0	200.0	10.0	464.0	7.0

external magnetic field. VSM measurements showed that there was no preferred in-plane magnetization direction. It should be pointed out that various microscopic origins might cause the increase of the damping factor, such as eddy current.[14]

The surface morphology of the Fe_3O_4/PR/Fe_3O_4 multilayer in Fig. 2(a) showed pebble-stone shaped particles with sizes ranging from a few hundred nanometers to a couple of microns. The magnitude of the complex reflection coefficients was recorded by SMM and is shown in Fig. 2(b). Prior to each SMM imaging, a frequency scan over the range of 0.5–6.0 GHz was performed, and typically a number of resonant peaks could be registered. To improve the accuracy and sensitivity, the SMM image was recorded in contact mode and in the vicinity of the sharpest resonance peaks (f = 2.3909 GHz). Compared to Fig. 2(a), there is a clear contrast between the inner grains and the boundaries in Fig. 2(b). The amplitude of the reflection coefficient from the grain boundaries is higher than those from the inner grain region, as manifested by bright lines for the grain boundaries and black holes for the grains. The surface morphology and the reflection coefficient were measured and read out through different channels (i.e., laser diode for surface morphology, PNA for SMM), ensuring decoupling between the surface morphology and the SMM image. The contrast in Fig. 2(b) thus reflects solely the response of RF/microwave signals due to the different electrical properties of the materials.

Measurements on a reference sample with known conductivity/resistivity were performed at the same frequency (Figs. 2(c) and 2(d)). The sample contained a 5 nm thick partially oxidized graphene nanosheet on a platinum surface. It is known that oxidized graphene has poorer conductivity than platinum. In Fig. 2(d), the platinum substrate appears to be brighter than the graphene oxide, suggesting that the grain boundaries are more conductive than the grains in Fig. 2(b).

An equivalent circuit of SMM is shown in Fig. 3(a). The shunt capacitive component represents the dielectric property, and the resistive component represents the conductivity of the sample. The length of the transmission line was designed to be $\lambda/2$ at ~2.5 GHz, where λ is the wavelength. Based on the transmission line theory, the amplitude $|\Gamma|$ and phase angle θ of the complex reflection coefficient can be written as

$$|\Gamma| = \frac{Z_0}{2} \cdot \sqrt{\frac{1}{R^2} + \omega^2 C^2}, \quad (1)$$

$$\theta = \tan^{-1}(\omega CR), \quad (2)$$

where ω is the angular frequency. From Eqs. (1) and (2), the sample with the higher electrical conductivity, i.e., the lower value of R, will have a larger value of $|\Gamma|$ and a smaller θ;

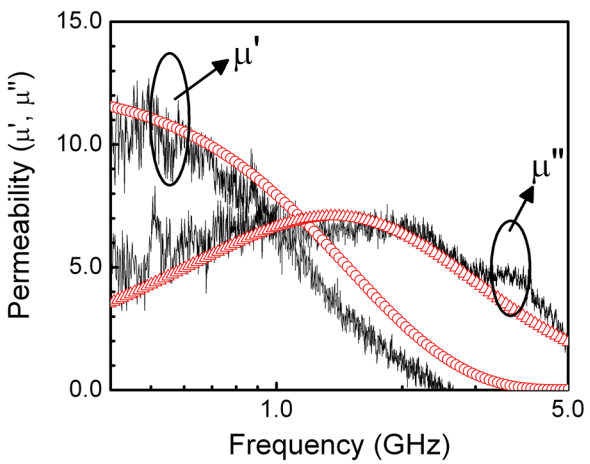

FIG. 1. (Color online) Measured and simulated complex permeability spectra of the Fe_3O_4/PR/Fe_3O_4 multilayer. The Landau-Lifshitz damping constant α was assumed to be ~0.46, and the other parameters used in the simulation are listed in Table I.

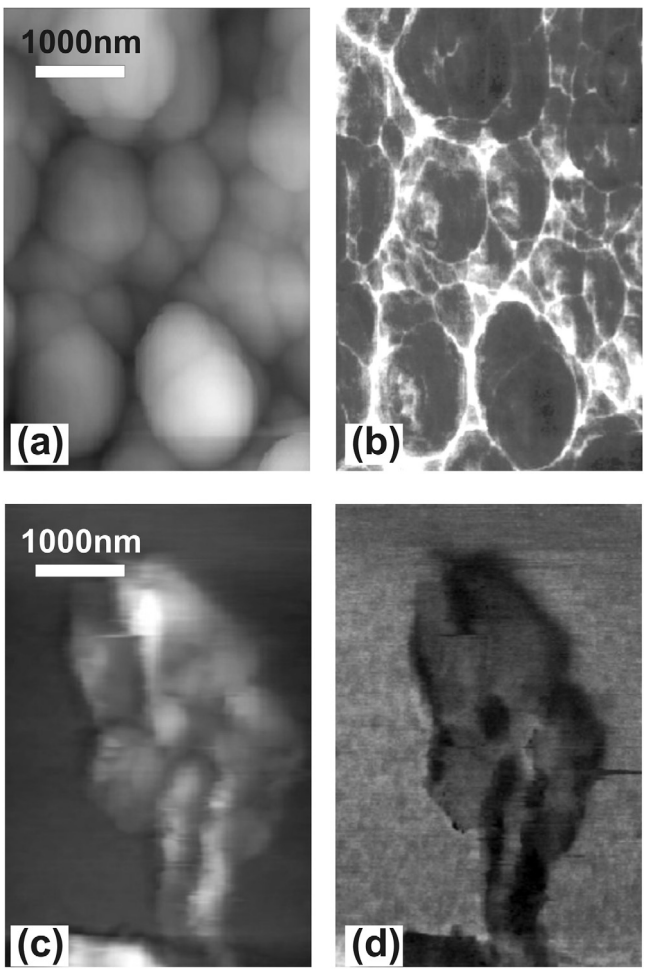

FIG. 2. (a) Surface morphology of the Fe_3O_4/PR/Fe_3O_4 multilayer, (b) amplitude of the reflection coefficient of the Fe_3O_4/PR/Fe_3O_4 multilayer by SMM recorded at 2.3909 GHz, (c) surface morphology of the graphene oxide/Pt sample, and (d) amplitude of the reflection coefficient of the graphene oxide/Pt sample by SMM recorded at 2.3909 GHz.

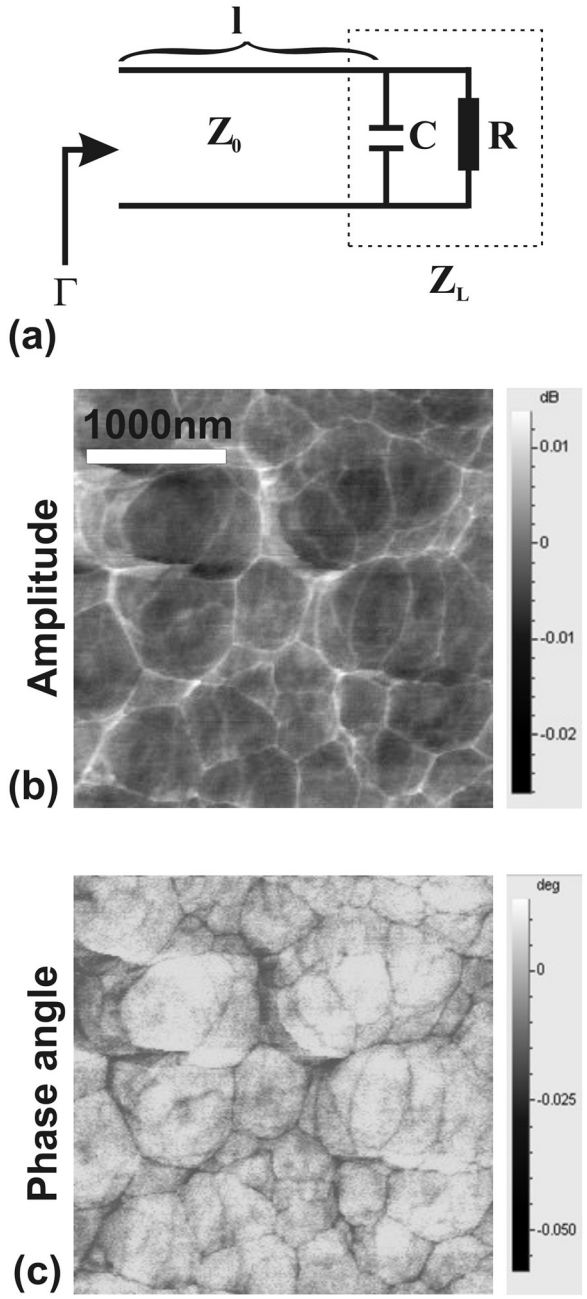

FIG. 3. (a) Equivalent circuit of SMM. (b) Amplitude and (c) phase angle of the reflection coefficient by SMM of the Fe_3O_4/PR/Fe_3O_4 recorded at $f = 2.4868$ GHz and $\theta = -93.388°$.

the sample with higher dielectric constant will have larger values of both $|\Gamma|$ and θ. Figure 3(b) and 3(c) show the measurements recorded at $\theta = -93.4°$ and $f = 2.4868$GHz. The grain boundary had a larger value of $|\Gamma|$ and a smaller value of θ, thus verifying a higher electrical conductivity of the grain boundary than of the grain. In practice, the $\lambda/2$ resonance was recognized by choosing the peak with a phase angle $\theta = -\pi/2$.

According to the grain-boundary space charge model, the mixed ionic and electronic boundary contains a grain boundary core and two adjacent space charge regions.[15–17] The accumulation of charges in the space charge region has been revealed by a number of groups.[18–20] The accumulated charges, we believe, play an important role in the enhancement of the local grain boundary conductivity, leading to the contrast in the SMM image. The excessive conductivity of the grain boundaries leads to significant eddy current and consequently increases the Landau-Lifshitz damping constant α.

IV. SUMMARY

In conclusion, we have performed *in situ* SMM characterization of multi-layer ferrite film prepared via low-temperature spin-spray processing. We discovered different electrical properties of the grain boundaries and the grains. The grain boundaries appeared to be more conductive, which might be caused by the charge accumulation in the grain boundary space charge region. The observation of excessive conductivity of the grain boundaries is in good agreement with our simulation results using a large value of α.

[1]B. Lax and K. J. Button, *Microwave Ferrites and Ferrimagnetics* (McGraw-Hill, New York, 1962), p. 145.
[2]Y. Zhuang, M. Vroubel, B. Rejaei, and J. N. Burghartz, Tech. Dig.—Int. Electron Devices Meet. **2002**, 475 (2011).
[3]M. Yamaguchi, T. Kuribara, and K. I. Arai, IEEE MTT-S Int. Microwave Symp. Dig. **1**, 197 (2002).
[4]V. Korenivski and R. B. Dover, IEEE Trans. Magn. **34**, 1375 (1998).
[5]P. S. Wang, H. Q. Zhang, R. Divan, and A. Hoffmann, IEEE Trans. Magn. **45**, 71 (2009).
[6]T. J. Klemmer, K. A. Ellis, L. H. Chen, B. van Dover, and S. Jin, J. Appl. Phys. **87**, 830 (2000).
[7]S. X. Wang, N. X. Sun, M. Yamaguchi, and S. Yabukami, Nature **407**, 150 (2000).
[8] K. Kondo, S. Yoshida, H. Ono, and M. Abe, J. Appl. Phys. **101**, 09M502 (2007).
[9]G. M. Yang, X. Xing, A. Daigle, M. Liu, O. Obi, J. W. Wang, K. Naishadham, and N. X. Sun, IEEE Trans. Magn. **44**, 3091 (2008).
[10]G. M. Yang, X. Xing, A. Daigle, M. Liu, O. Obi, S. Stoute, K. Naishadham, and N. X. Sun, IEEE Trans. Antennas Propag. **57**, 2190 (2009).
[11]S. Wu and J. J. Yu, Appl. Phys. Lett. **97**, 202902 (2010).
[12]I. Humer, O. Bethge, M. Bodnarchuk, M. Kovalenko, M. Yarema, W. Heiss, H. P. Huber, M. Hochleitner, P. Hinterdorfer, F. Kienberger, and J. Smoliner, J. Appl. Phys. **109**, 064313 (2011).
[13]J. Smoliner, H. P. Huber, M. Hochleitner, M. Moertelmaier, and F. Kienberger, J. Appl. Phys. **108**, 064315 (2010).
[14]J. R. Bosnell, J. Phys. D: Appl. Phys. **1**, 1389 (1968).
[15]X. Guo and R. Waser, Prog. Mater. **51**, 151 (2006).
[16]H. L. Tuller, Solid State Ionics **131**, 143 (2000).
[17]S. Kim and J. Maier, J. Electrochem. Soc. **149**, J73 (2002).
[18]T. H. Estell and S. N. Flengas, Chem. Rev. **70**, 339 (1970).
[19]S. S. Liou and W. L. Worrell, Appl. Phys. A: Solids Surf. **49**, 25 (1989).
[20]F. Capel, C. Moure, and P. Duran, J. Mater. Sci. **35**, 345 (2000).